

## Magic wavelengths for the 6S-7P transition of cesium atoms

Jiandong Bai<sup>a,b</sup>, Yang Liu<sup>a</sup>, Shaofeng Fan<sup>a</sup>, Shuo Liu<sup>c</sup>, Wenyuan Liu<sup>a</sup>, Qi Jie<sup>a</sup>, Yijun Li<sup>a</sup>, Junmin Wang<sup>b,d,\*</sup>

<sup>a</sup> Department of Physics, North University of China, Taiyuan 030051, China

<sup>b</sup> State Key Laboratory of Quantum Optics and Quantum Optics Devices, and Institute of Opto-Electronics, Shanxi University, Taiyuan 030006, China

<sup>c</sup> Center for Optics Research and Engineering, Shandong University, Qingdao 266000, China

<sup>d</sup> Collaborative Innovation Center of Extreme Optics, Shanxi University, Taiyuan 030006, China

### ARTICLE INFO

#### Keywords:

Dynamic polarizability  
Optical dipole trap  
Magic wavelength  
Robustness

### ABSTRACT

For the trapped pre-cooled atoms in an optical dipole trap (ODT), the magic-wavelength ODT can eliminate the differential light shift of the transition between two atomic states, so that the transition frequency between the two states is the same as that of atoms in the free space, which is of great significance for improving the experimental repetition rate and reducing the atomic decoherence in the fields of cold atom physics, quantum optics, and precision measurement. Here we calculate the dynamic polarizabilities of cesium 6S ground state and 7P excited state by using the multi-level model for the ODT with laser wavelength from 1200 to 2000 nm. The magic wavelengths of ODT are obtained for the linearly and circularly polarized laser beams at the intersection of dynamic polarizabilities of two atomic states. Furthermore, we analyze the robustness of the magic trapping conditions and the feasibility of the experimental operation near the telecom C-band wavelength.

### Introduction

Laser cooling and trapping of neutral atoms is of great significance for studying the physical and chemical properties of atoms. To further realize spatial localization of atoms and manipulate individual atoms, ions or molecules, the optical dipole trap (ODT) [1] was proposed and widely used in cold atom physics, quantum optics, precision measurement and other fields. For rubidium, cesium, and strontium atoms, the 532-nm and 1064-nm far-detuned ODTs [2–4] are used in experiments because such commercial lasers have stable performance and mature technology. However, the ODTs' laser wavelengths are commonly not magic, it will inevitably seriously affect the central frequency of the concerned atomic transition, especially for the coherent manipulation of atomic internal states and the study of new optical atomic clocks. In order to eliminate the AC Stark shift of desired atomic transition associated with the spatial distribution of light intensity in ODTs, the ODTs can be turned off during excitation/radiation. But this method will shorten the atomic trapping lifetime and reduce the experimental repetition rate. The AC Stark shift can be experimentally eliminated by constructing blue-detuned dark ODTs [5], but the micron-level dark ODTs usually require more complex experimental equipment and are difficult to operate. The above mentioned issues can be solved with a

magic-wavelength ODT [6–8], which can make the AC Stark shifts of the upper and lower states of the atoms exactly the same. It is of great significance to improve the repetition rate of experimental sequences and weaken the atomic decoherence [9].

When the differential light shift of the transition between two atomic states is zero, the trapping laser wavelength is called magic wavelength. It has been experimentally realized and well applied in the research of strontium atom, ytterbium atom, and mercury atomic clocks [10–12], and so on. It is very important to improve the stability and accuracy of atomic clock. Traditional cesium cold atom experiments are carried out in a magneto-optical trap based on 6S-6P cooling transition. Comparing with the 6P state, the 7P state level has the relatively longer spontaneous radiation lifetime and the corresponding natural linewidth is narrower. Recently, Graham et al. demonstrated multi-qubit entanglement and algorithms on a neutral-atom quantum computer in a ladder-type three-level system of Cs  $6S_{1/2}$ - $7P_{1/2}$ - $7S_{1/2}$  transition based on the narrow spectral linewidth [13]. And the 6S- $n$ P transitions are significant to the test of the Standard Model [14]. In 2016, Safronova et al. used the relativistic high-precision all-order method to calculate the dynamic polarizabilities of cesium 6S and 7P states and the corresponding magic wavelengths, but only for linearly polarized light [15].

In this paper, we calculate the dynamic polarizabilities of cesium 6S

\* Corresponding author.

E-mail address: [wjmm@sxu.edu.cn](mailto:wjmm@sxu.edu.cn) (J. Wang).

<https://doi.org/10.1016/j.rinp.2023.106853>

Received 12 July 2023; Received in revised form 6 August 2023; Accepted 11 August 2023

Available online 12 August 2023

2211-3797/© 2023 The Authors. Published by Elsevier B.V. This is an open access article under the CC BY-NC-ND license (<http://creativecommons.org/licenses/by-nc-nd/4.0/>).

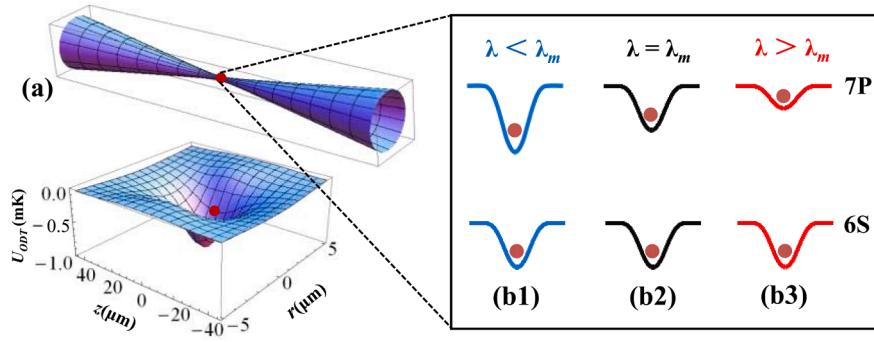


Fig. 1. (a) An ODT formed by focusing a single-mode Gaussian laser beam is used to trap atoms; (b) Light shifts of the 6S and 7P states near the magic wavelength  $\lambda_m$ .

ground state and 7P excited state by using the multi-level model in the wavelength range of 1200–2000 nm. The magic trapping wavelengths in the ODT are obtained for the linearly and circularly polarized lights. Furthermore, we analyze the robustness of the magic trapping conditions for laser wavelength near the telecom C-band wavelength.

### Theoretical methods

In order to achieve a longer trapping lifetime of atoms and maintain the coherence of their internal states, atoms can usually be trapped in an ODT. When the atoms interact with the optical field, the optical field will induce the atom to produce the electric dipole moment, and its interaction potential can be expressed as [16]

$$U = -\alpha(\omega) \frac{P}{\epsilon_0 c \pi w_0^2} \quad (1)$$

where  $P$  and  $w_0$  are the average power and the waist spot radius at the waist position of incident ODT laser, respectively.  $\epsilon_0$  and  $c$  are the dielectric constant and the speed of light in vacuum. The interaction potential  $U$  is proportional to the atomic polarizability  $\alpha(\omega)$ , and it is a dipole potential. Thus, the atom is subjected to a dipole force generated by the gradient of the dipole potential, which can trap it in the ODT, as shown in Fig. 1. When the wavelength of the ODT laser is greater than or less than the magic wavelength ( $\lambda > \lambda_m$  or  $\lambda < \lambda_m$ ), the depth of the potential well formed by the same laser for the ground state and the excited state is different, which will lead to the photon transition between the two atomic states depending on the spatial position of the optical field, as shown in Fig. 1(b1) and Fig. 1(b3). However, when the wavelength of the far-red detuned ODT formed by a single-mode Gaussian laser beam is magic wavelength ( $\lambda = \lambda_m$ ), the photon transition does not depend on the differential light shift between the two atomic states (Fig. 1(b2)).

Thus, in order to find the magic wavelength, we must calculate the dynamic polarizabilities  $\alpha(\omega)$  of two target atomic states.  $\alpha(\omega)$  describes the degree of deviation from normal distribution of electron cloud of atoms or molecules under the action of external electric field, which is expressed as [17]:

$$\alpha_i(\omega) = \alpha_i^S(\omega) + A \cos \theta_k \frac{m_{ji}}{2j_i} \alpha_i^Y(\omega) + \left( \frac{3 \cos^2 \theta_p - 1}{2} \right) \frac{3m_{ji}^2 - j_i(j_i + 1)}{j_i(2j_i - 1)} \alpha_i^T(\omega) \quad (2)$$

where  $A$  represents the degree of circular polarization.  $j$  and  $m_j$  represent the total angular momentum quantum number and magnetic quantum number, respectively.  $\theta_k$  and  $\theta_p$  are required to satisfy the geometric relation  $\cos^2 \theta_k + \cos^2 \theta_p \leq 1$ .  $\alpha_i^S(\omega)$ ,  $\alpha_i^Y(\omega)$ , and  $\alpha_i^T(\omega)$  represent scalar, vector and tensor polarizabilities, respectively, which are expressed as [17]

$$\begin{aligned} \alpha_i^S(\omega) &= \sum_n \frac{f_{in}}{\Delta E_{ni}^2 - \omega^2} + \alpha_{core} \\ \alpha_i^Y(\omega) &= -3 \sqrt{\frac{6j_i(2j_i + 1)}{j_i + 1}} \sum_n (-1)^{j_n + j_i} \begin{Bmatrix} 1 & 1 & 1 \\ j_i & j_i & j_n \end{Bmatrix} \frac{f_{in}}{\Delta E_{ni}^2 - \omega^2} \frac{\omega}{\Delta E_{ni}} \\ \alpha_i^T(\omega) &= 6 \sqrt{\frac{5j_i(2j_i - 1)(2j_i + 1)}{6(j_i + 1)(2j_i + 3)}} \sum_n (-1)^{j_n + j_i} \begin{Bmatrix} 1 & 1 & 2 \\ j_i & j_i & j_n \end{Bmatrix} \frac{f_{in}}{\Delta E_{ni}^2 - \omega^2} \end{aligned} \quad (3)$$

here,  $\alpha_{core}$  represents the nuclear polarizability of atoms, which almost does not change with the laser frequency and is approximately regarded as a constant [18]. In this paper, the units of polarizability are the atomic unit system, that is, “a.u.” stands for “atomic units”. For cesium atom,  $\alpha_{core} = 15.81$  a.u. The oscillator strength is defined as

$$f_{in} = \frac{2\Delta E_{ni}}{3(2j_i + 1)} |\langle \psi_i || r C^1(\hat{r}) || \psi_n \rangle|^2 \quad (4)$$

here,  $\Delta E_{ni} = E_n - E_i$  and  $\langle \psi_i || r C^1(\hat{r}) || \psi_n \rangle$  are the transition energy and the reduced matrix element from the  $|\psi_n\rangle$  state to the  $|\psi_i\rangle$  state, respectively.  $C^1(\hat{r})$  is the first-order spherical tensor. These values can be found from Refs. [19,20].

In Eq. (3), the polarizability of  $|\psi_i\rangle$  state is contributed from all the other  $|\psi_n\rangle$  state which satisfy the electric dipole transition selection rule [21,22]. Because the photon transition energy from the highly-excited state to the ground state and the low-excited state is large and the matrix element of the electric dipole transition is small, the contribution of the highly-excited state to its polarizability is very small. As a result, we calculate the dynamic electric polarizabilities of Cs 6S<sub>1/2</sub> ground state and 7P<sub>3/2</sub> excited state based on multi-level model, where the maximum value of the principal quantum number  $n$  of  $|\psi_n\rangle$  is 20. For 6S<sub>1/2</sub> state, its polarizability is from the contribution of P<sub>1/2</sub> and P<sub>3/2</sub> states in the range of  $n = 6 - 20$ . For 7P<sub>1/2</sub> state, the contribution of S<sub>1/2</sub> and D<sub>3/2</sub> states should be taken into account. For 7P<sub>3/2</sub> state, the contribution of S<sub>1/2</sub>, D<sub>3/2</sub>, and D<sub>5/2</sub> states should be taken into account. In this case, the lower limit of principal quantum number of S and D states are  $n = 6$  and  $n = 4$ , respectively.

## Results and discussion

### A. Magic wavelengths for the 6S<sub>1/2</sub> – 7P<sub>1/2</sub> transition

In the paper, we calculate the polarizabilities of the 6S and 7P states in the case of  $|\cos \theta_k|^2 = 1$  and  $|\cos \theta_p|^2 = 0$ . For atomic states with an angular momentum quantum number equal to 0.5, there is no tensor polarizability. Thus, the polarizabilities of the 6S<sub>1/2</sub> and 7P<sub>1/2</sub> states can be expressed as

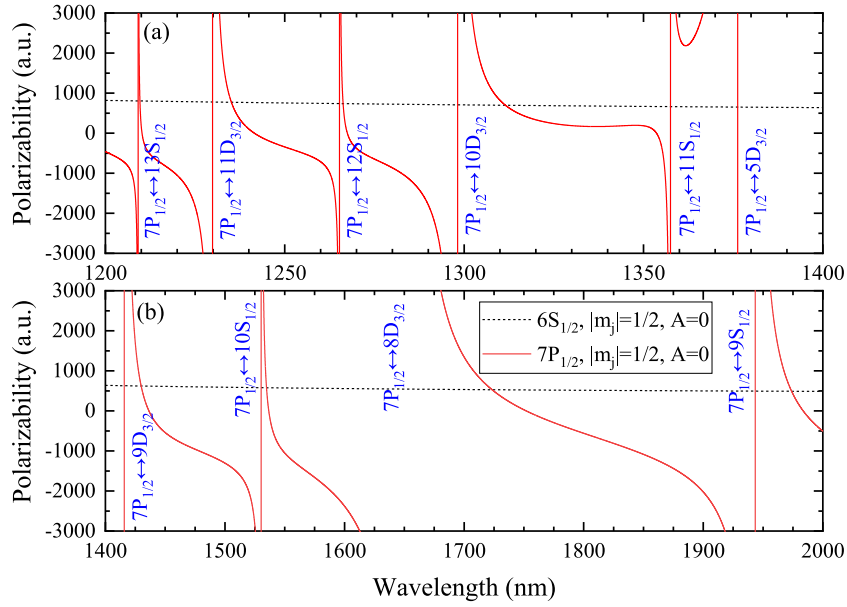


Fig. 2. Dynamic polarizabilities of Cs  $6S_{1/2}$  and  $7P_{1/2}$  states in the range of 1200 – 2000 nm for linearly polarized light ( $A = 0$ ).

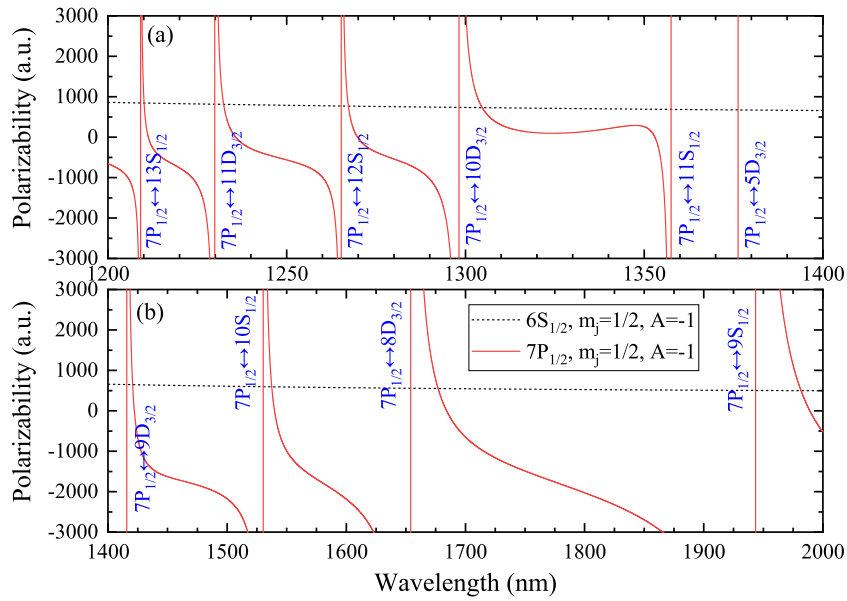


Fig. 3. Dynamic polarizabilities of Cs  $6S_{1/2}$  and  $7P_{1/2}$  states in the range of 1200 – 2000 nm for left-handed circularly polarized light ( $A = -1$ ).

$$\alpha_i(\omega) = \alpha_i^S(\omega) + A \frac{m_{ji}}{2j_i} \alpha_i^V(\omega) \quad (5)$$

The dynamic polarizabilities of the  $6S_{1/2}$  and  $7P_{1/2}$  states are shown in Figs. 2-4 for linearly ( $A = 0$ ) and circularly ( $A = \pm 1$ ) polarized lights in the range of 1200–2000 nm. The black dashed line and red solid line represent the dynamic polarizabilities of the ground state and the excited state, respectively. The abscissa corresponding to the intersection of their polarizabilities is called magic wavelength, where the polarizabilities of the two states are equal. The potential depths of the ODT formed by a focused single-mode Gaussian laser beam are same, as shown in Fig. 1(b). Near the magic wavelength  $\lambda_m$ , when the laser wavelength is smaller than the magic wavelength, the potential well depth of the excited state is greater than that of the ground state. Conversely, when the laser wavelength is larger than the magic wavelength, the potential well depth of the excited state is less than that of the ground state. In either case, the differential light shift between the two

atomic states will be non-zero. This spatially position-dependent differential light shift will heat the atoms and push them out of the potential well, resulting in rapid decoherence. However, these issues can be solved well when the wavelength of the trapping laser meets the magic condition.

For linearly and left-handed circularly polarized lights, there are eight magic wavelengths in the range of 1200–2000 nm. However, for right-handed circularly polarized light, only four magic wavelengths exist in the same range. That is, there is no magic wavelength near the  $7P_{1/2} \leftrightarrow nS_{1/2}$  transition. The magic wavelengths and polarizabilities of the  $6S_{1/2}$ - $7P_{1/2}$  transition for linearly and circularly polarized lights are listed in Table 1.

#### B. Magic wavelengths for the $6S_{1/2} - 7P_{3/2}$ transition

Due to angular momentum quantum number  $j = 1.5$ , the total

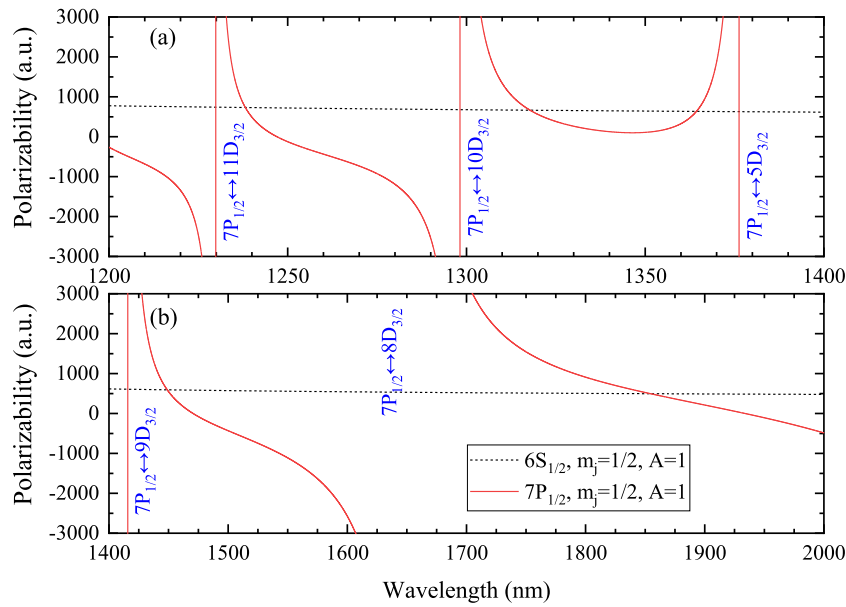


Fig. 4. Dynamic polarizabilities of Cs  $6S_{1/2}$  and  $7P_{1/2}$  states in the range of 1200 – 2000 nm for right-handed circularly polarized light ( $A = 1$ ).

Table 1

The magic wavelengths (in nm) and the corresponding polarizabilities (in a.u.) of the  $6S_{1/2}$ - $7P_{1/2}$  transition for linearly and circularly polarized lights.

Resonance transitions	$\lambda_{\text{res}}$	$A = 0$		$A = -1$		$A = 1$	
		$\lambda_{\text{magic}}$	$\alpha_{\text{magic}}$	$\lambda_{\text{magic}}$	$\alpha_{\text{magic}}$	$\lambda_{\text{magic}}$	$\alpha_{\text{magic}}$
$7P_{1/2}$ - $13S_{1/2}$	1209.13						
$7P_{1/2}$ - $11D_{3/2}$	1229.86	1209.63	803.01	1210.10	844.09		
$7P_{1/2}$ - $12S_{1/2}$	1265.27	1235.13	770.75	1232.36	813.42	1238.15	733.60
$7P_{1/2}$ - $10D_{3/2}$	1298.21	1266.27	738.04	1267.26	767.13		
$7P_{1/2}$ - $11S_{1/2}$	1357.52	1311.52	696.13	1304.69	727.52	1317.74	666.95
$7P_{1/2}$ - $5D_{3/2}$	1376.26					1364.33	631.85
$7P_{1/2}$ - $9D_{3/2}$	1415.76	1429.90	624.39	1420.70	645.72	1448.81	596.11
$7P_{1/2}$ - $10S_{1/2}$	1530.25	1534.75	579.20	1537.45	593.57		
$7P_{1/2}$ - $8D_{3/2}$	1654.02	1723.33	532.56	1677.01	552.40	1854.32	496.86
$7P_{1/2}$ - $9S_{1/2}$	1943.52	1973.85	494.34	1981.63	498.71		

polarizability of the  $7P_{3/2}$  states includes a tensor component, which is expressed as

$$\alpha_i(\omega) = \alpha_i^s(\omega) + A \frac{m_{j_i} \alpha_i^v(\omega)}{2j_i} - \frac{3m_{j_i}^2 - j_i(j_i + 1)}{2j_i(2j_i - 1)} \alpha_i^T(\omega) \quad (6)$$

The dynamic polarizabilities of the  $6S_{1/2}$  and  $7P_{3/2}$  states are shown in Figs. 5-7 for linearly ( $A = 0$ ) and circularly ( $A = \pm 1$ ) polarized lights in the range of 1200–1900 nm. The black dashed line and solid lines represent the dynamic polarizabilities of the ground state and the excited state, respectively. It is different from the  $7P_{1/2}$  state that it has 4 angular momentum magnetic quantum numbers  $m_j = \pm 1/2, \pm 3/2$ . Because the two cases for  $A = 1, m_j = 1/2$  and  $A = -1, m_j = -1/2$  (or  $A = 1, m_j = 3/2$  and  $A = -1, m_j = -3/2$ ) are equivalent, we only analysis the dynamic polarizabilities of  $7P_{3/2}, m_j = 1/2, 3/2$ . Therefore, there are two magic wavelengths near each resonant transition.

For linearly and left-handed circularly polarized lights, there are sixteen magic wavelengths in the range of 1200–1900 nm near the  $7P_{3/2} \leftrightarrow nS_{1/2}, nD_{3/2,5/2}$  transitions. However, for right-handed circularly

polarized light, there is no magic wavelength near the  $7P_{3/2} \leftrightarrow nS_{1/2}$  transition. The magic wavelengths and polarizabilities of the  $6S_{1/2} \leftrightarrow 7P_{3/2}, m_j = 1/2$  and  $3/2$  transitions for linearly and circularly polarized lights are listed in Table 2 and Table 3.

### C. The robustness of the magic condition

In order to evaluate the robustness of magic ODT, we calculate the ratio of the depth difference and itself of the potential well between the  $6S_{1/2}$  ground state and the  $7P_{1/2}$  excited state with the offset of the wavelength of ODT laser relative to the magic wavelength, as shown in Fig. 8. The blue and red curves show that the relative change rate of the potential well varies with the laser wavelength offset near 1534.75 nm and 1537.45 nm, respectively. Compared with the 1534.75-nm magic ODT, the relative change rate of the dipole potential of the 1537.45-nm magic ODT is smaller within  $\pm 6\%$  in the range of  $\pm 0.1$  nm. When the change of the ODT laser wavelength is  $\pm 0.01$  nm, the relative change rate of the dipole potential of the 1537.45-nm magic ODT is only less than  $\pm 0.6\%$ , thus its robustness is better.

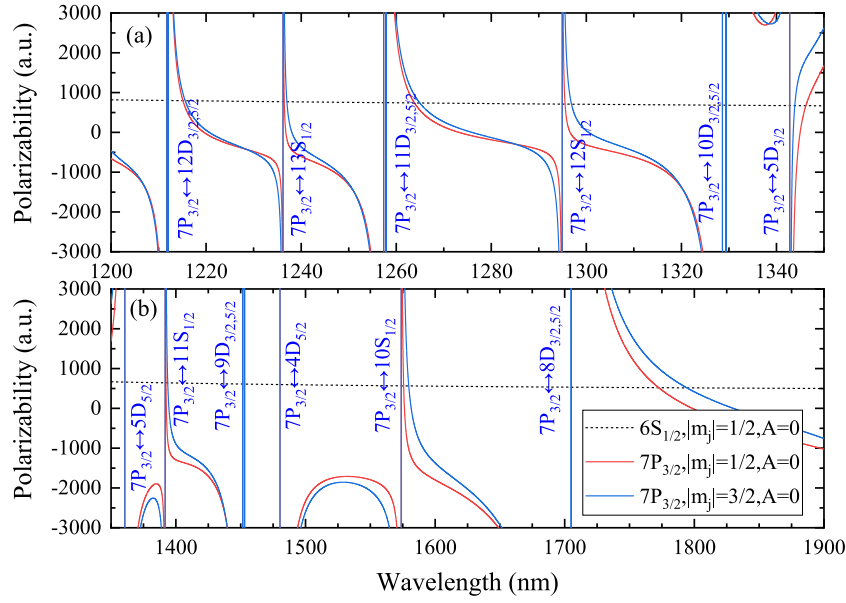


Fig. 5. Dynamic polarizabilities of Cs  $6S_{1/2}$  and  $7P_{3/2}$  states in the range of 1200 – 2000 nm for linearly polarized light ( $A = 0$ ).

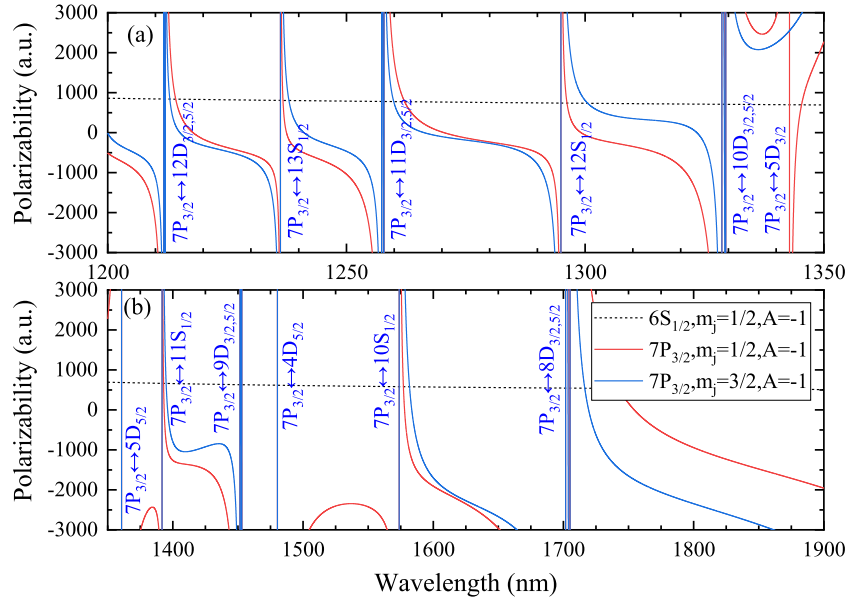


Fig. 6. Dynamic polarizabilities of Cs  $6S_{1/2}$  and  $7P_{3/2}$  states in the range of 1200 – 2000 nm for left-handed circularly polarized light ( $A = -1$ ).

Fig. 9 shows the robustness of the magic ODT for trapping the  $6S_{1/2}$  ground state and the  $7P_{3/2}$  excited state near the telecom C-band wavelength. The relative change rates of the dipole potential of the 1579.67-nm and 1581.79-nm magic ODTs are almost identical, less than  $\pm 7\%$  in the range of  $\pm 0.1$  nm. And they are far less than that of the 1575.73-nm and 1577.08-nm magic-wavelength ODTs. When the wavelength change of the ODT laser is  $\pm 0.01$  nm, the relative change rates of the dipole potential of the 1579.67-nm and 1581.79-nm magic ODTs are only less than  $\pm 0.7\%$ , thus their robustness are better.

The typical well depth of the conventional optical lattice is about 10–100Er, which can be expressed as

$$U = k_B T = n E_r \quad (7)$$

where  $k_B$  is the Boltzmann constant;  $E_r = \hbar^2 / (2m\lambda^2)$  is the single-photon recoil energy,  $\hbar$  is Planck's constant,  $m$  is the mass of a single atom, and  $\lambda$  is the cooling transition wavelength; When the well depths of the optical

lattice are 50Er and 100Er, the corresponding temperature  $T$  is about 5 and 10  $\mu\text{K}$ . By substituting the above parameters into Eq. (7), the relationship between the required laser power of the optical well and the radius of the waist spot at the location of the beam waist can be obtained for better robustness magic-wavelength ODTs at 1537.45, 1579.66, and 1581.79 nm, as shown in Fig. 10. The larger the beam waist is, the higher the power of the trapping laser is required. When the beam waist is the same, the higher laser power is required for the deeper potential well. Typically, when an optical trap with a depth of 100Er is formed, the required laser power are about 996, 1074, and 1048 mW for these magic wavelengths of 1537.45, 1579.66, and 1581.79 nm with the beam waist radius of 50  $\mu\text{m}$ .

Because the ODT laser traps atoms in the strongest position of light intensity, it will inevitably cause strong photon scattering. In order to evaluate the trapping lifetime of atoms in the optical trap, we calculate the photon scattering rate caused by the magic-wavelength laser with a

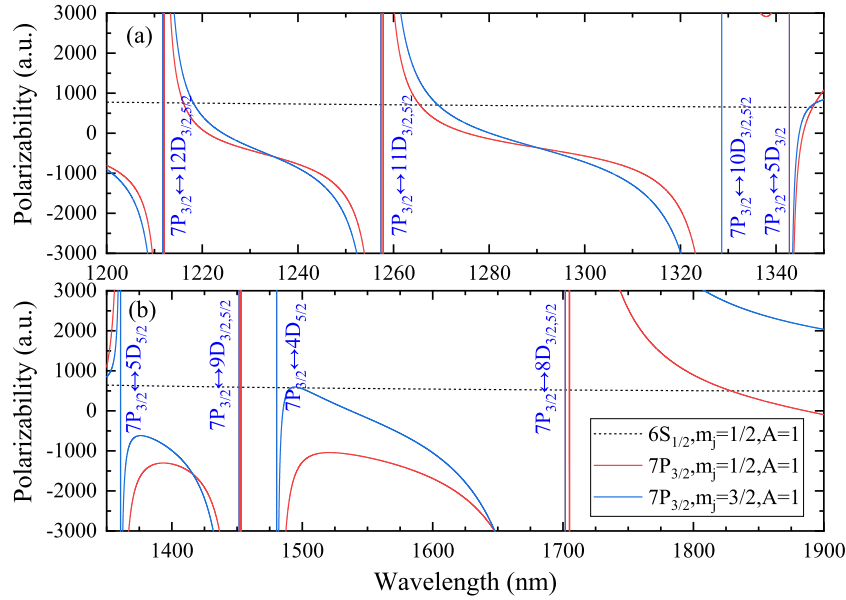


Fig. 7. Dynamic polarizabilities of Cs  $6S_{1/2}$  and  $7P_{3/2}$  states in the range of 1200 – 2000 nm for right-handed circularly polarized light ( $A = 1$ ).

Table 2

The magic wavelengths (in nm) and the corresponding polarizabilities (in a.u.) of the  $6S_{1/2}$ - $7P_{3/2}$ ,  $m_j = 1/2$  transition for linearly and circularly polarized lights.

Resonance transitions	$\lambda_{res}$	A = 0		A = -1		A = 1	
		$\lambda_{magic}$	$\alpha_{magic}$	$\lambda_{magic}$	$\alpha_{magic}$	$\lambda_{magic}$	$\alpha_{magic}$
$7P_{3/2}$ - $12D_{5/2}$	1211.72						
$7P_{3/2}$ - $12D_{3/2}$	1212.06	1212.01	800.91	1211.98	841.19	1212.03	760.71
$7P_{3/2}$ - $13S_{1/2}$	1236.19	1215.13	796.7	1214.24	837.69	1216.05	755.96
$7P_{3/2}$ - $11D_{5/2}$	1257.36	1236.45	769.75	1236.71	805.73	1257.82	712.38
$7P_{3/2}$ - $11D_{3/2}$	1257.87	1257.79	745.81	1257.74	779.32	1265.48	705.37
$7P_{3/2}$ - $12S_{1/2}$	1294.93	1263.83	739.54	1262.19	774.09	1329.37	655.96
$7P_{3/2}$ - $10D_{5/2}$	1328.63	1295.53	709.56	1296.2	738.19		
$7P_{3/2}$ - $10D_{3/2}$	1329.45	1329.33	682.3	1329.26	708.67		
$7P_{3/2}$ - $5D_{3/2}$	-1342.80	1346.19	670.16	1345.32	695.96	1347.66	644.21
$7P_{3/2}$ - $5D_{5/2}$	-1360.63						
$7P_{3/2}$ - $11S_{1/2}$	1391.72	1392.38	641.17	1392.9	662.94	1452.85	591.28
$7P_{3/2}$ - $9D_{5/2}$	1451.51	1452.77	610.45	1452.65	629.64		
$7P_{3/2}$ - $9D_{3/2}$	1453.01						
$7P_{3/2}$ - $4D_{5/2}$	-1480.39						
$7P_{3/2}$ - $10S_{1/2}$	1573.85	1575.73	564.84	1577.08	579.43		
$7P_{3/2}$ - $8D_{5/2}$	1701.70	1704.54	532.23	1704.23	544.59	1704.72	519.91
$7P_{3/2}$ - $8D_{3/2}$	1705.08	1772.49	519.01	1716.36	541.85	1828.7	499.23

depth of 50Er and 100Er near the 1.55- $\mu$ m band, which are listed in Table 4 The photon scattering rate can be expressed as[16]

$$\Gamma_{sc}(r) = \frac{6\pi c^2}{\hbar\omega_{res}} \left(\frac{\omega_m}{\omega_{res}}\right)^2 \left(\frac{\Gamma}{\omega_{res}^2 - \omega_m^2}\right)^2 I(r) \quad (8)$$

where  $\omega_{res}$  and  $\omega_m$  are the angular frequencies of resonant transition and magic-wavelength laser,  $I(r)$  is the laser intensity distribution.  $\Gamma$  is the spontaneous and induced transitions rates.

Table 4 shows that the photon scattering rate decreases with the

increase of the difference between magic wavelength and resonance wavelength. The photon scattering of the 1537.45-nm magic-wavelength ODT is minimum. And it also has a lower rate of change in potential well, as discussed above. Moreover, considering the commercial watt-level high-power fiber laser system[23] and frequency locking technology[24] in the telecom C-band wavelength, the magic-wavelength ODT formed by the 1537.45-nm single-mode Gaussian laser beam have potential application in quantum computing and quantum simulation based on multi-atom array or optical lattice.

**Table 3**

The magic wavelengths (in nm) and the corresponding polarizabilities (in a.u.) of the  $6S_{1/2}-7P_{3/2}$ ,  $m_j = 3/2$  transition for linearly and circularly polarized lights.

Resonance transitions	$\lambda_{\text{res}}$	A = 0		A = -1		A = 1	
		$\lambda_{\text{magic}}$	$\alpha_{\text{magic}}$	$\lambda_{\text{magic}}$	$\alpha_{\text{magic}}$	$\lambda_{\text{magic}}$	$\alpha_{\text{magic}}$
$7P_{3/2}-12D_{5/2}$	1211.72	1212.04	800.89	1211.90	841.31		
$7P_{3/2}-12D_{3/2}$	1212.06	1215.59	796.08	1213.01	839.58	1218.15	753.54
$7P_{3/2}-13S_{1/2}$	1236.19	1236.99	769.10	1237.96	804.05		
$7P_{3/2}-11D_{5/2}$	1257.36	1257.84	745.79	1257.64	779.44		
$7P_{3/2}-11D_{3/2}$	1257.87	1264.96	738.39	1259.9	776.78	1269.32	701.94
$7P_{3/2}-12S_{1/2}$	1294.93	1296.88	708.37	1300.54	734.04		
$7P_{3/2}-10D_{5/2}$	1328.63	1329.41	682.24	1329.13	708.78		
$7P_{3/2}-10D_{3/2}$	1329.45						
$7P_{3/2}-5D_{3/2}$	-1342.80	1343.86	671.82			1347.03	644.63
$7P_{3/2}-5D_{5/2}$	-1360.63						
$7P_{3/2}-11S_{1/2}$	1391.72	1393.74	640.4	1394.87	661.69		
$7P_{3/2}-9D_{5/2}$	1451.51	1452.92	610.38	1452.40	629.77		
$7P_{3/2}-9D_{3/2}$	1453.01						
$7P_{3/2}-4D_{5/2}$	-1480.39					1491.64	576.38
						1498.05	574.05
$7P_{3/2}-10S_{1/2}$	1573.85	1579.66	563.64	1581.79	577.89		
$7P_{3/2}-8D_{5/2}$	1701.70	1704.87	532.16	1703.48	544.76		
$7P_{3/2}-8D_{3/2}$	1705.08	1794.21	515.25	1742.38	536.26		

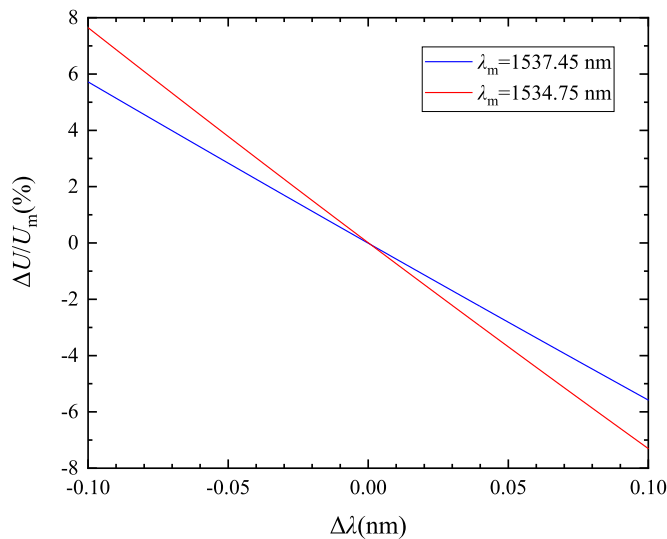


**Fig. 8.** For the  $6S_{1/2}$  ground state and  $7P_{1/2}$  excited state, the relative potential well depth varies with the laser wavelength forming the magic ODT.

**Conclusion**

In summary, we calculate the dynamic polarizabilities of the  $6S_{1/2}$  ground state and  $7P_{1/2,3/2}$  excited states of cesium atom by using the multi-level model, and identify the magic wavelengths for trapping the two states for the linearly and circularly polarized lights. In the wavelength range of 1200–2000 nm, there are multiple magic wavelengths. Then we analyze and discuss the advantages and disadvantages of different light traps and the robustness of magic-wavelength trapping

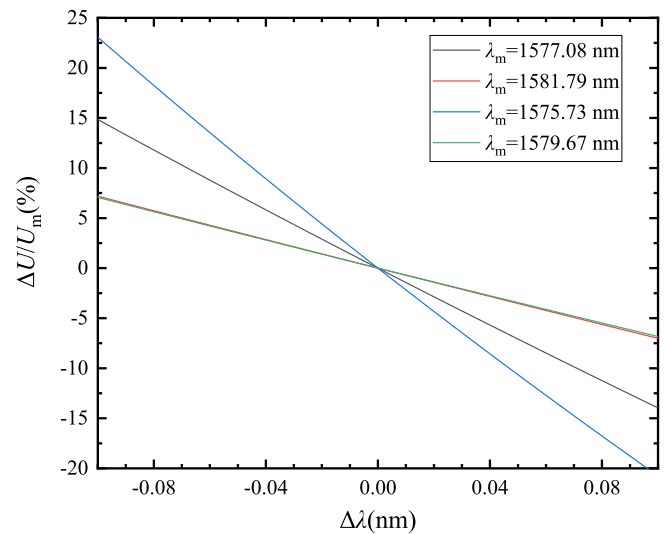


**Fig. 9.** For the  $6S_{1/2}$  ground state and  $7P_{3/2}$  excited state, the relative potential well depth varies with the laser wavelength forming the magic ODT.

conditions near the telecom C-band wavelength for the transitions of  $6S_{1/2} - 7P_{1/2}$  and  $6S_{1/2} - 7P_{3/2}$ , respectively. Near the telecom C-band wavelength, there are two and four magic wavelengths for the transitions of  $6S_{1/2} - 7P_{1/2}$  and  $6S_{1/2} - 7P_{3/2}$ , respectively. We find that the magic-wavelength ODT formed by the 1537.45-nm focused single-mode Gaussian laser beam have better robustness. Considering the commercial fiber laser and fiber amplifier in the telecom C-band wavelength, the high-precision ultra-stable cavity and frequency locking technology, these analysis can provide useful reference for the design and

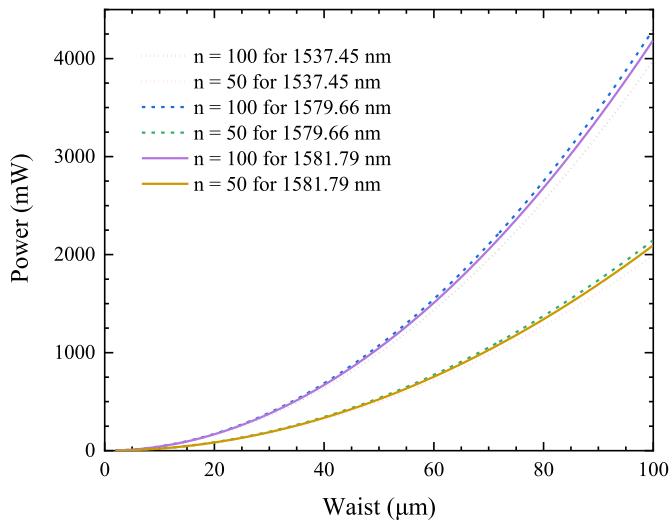


**Fig. 10.** When the well depths of the ODT are 50Er and 100Er, the required power of the ODT laser varies with the beam waist radius for these magic wavelengths of 1537.45, 1579.66, and 1581.79 nm.

**Table 4**

The photon scattering rates caused by a magic-wavelength ODT laser with a depth of 50Er and 100Er near the 1.55- $\mu\text{m}$  band.

$\lambda_{\text{res}}$ (nm)	$\lambda_{\text{magic}}$ (nm)	$\alpha_{\text{magic}}$ (a.u.)	$\Gamma_{\text{sc}} (\text{s}^{-1})_{50\text{Er}}$	$\Gamma_{\text{sc}} (\text{s}^{-1})_{100\text{Er}}$
1530.25	1534.75	579.20	39.77	69.54
	1537.45	593.57	13.25	26.50
1573.85	1575.73	564.84	760.35	1520.69
	1577.08	579.43	251.10	502.20
	1579.66	563.64	79.87	159.74
	1581.79	577.89	41.70	83.40

construction of Cs magic trap experiment, and has important application value in the fields of quantum computing, quantum simulation and quantum precision measurement.

#### CRediT authorship contribution statement

**Jiandong Bai:** Conceptualization, Methodology, Software, Investigation, Formal analysis, Funding acquisition, Writing – original draft. **Yang Liu:** Investigation, Visualization. **Shaofeng Fan:** Resources, Data curation. **Shuo Liu:** Resources, Writing – review & editing. **Wenyuan Liu:** Software, Validation, Funding acquisition. **Qi Jie:** Visualization, Funding acquisition. **Yijun Li:** Visualization, Supervision. **Junmin Wang:** Conceptualization, Funding acquisition, Resources, Supervision, Writing – review & editing.

#### Declaration of Competing Interest

The authors declare that they have no known competing financial interests or personal relationships that could have appeared to influence the work reported in this paper.

#### Data availability

Data will be made available on request.

#### Acknowledgements

This project was funded by the National Key R&D Program of China (2021YFA1402002), the National Natural Science Foundation of China (12104417, 12104419, 11974226), and the Fundamental Research Program of Shanxi Province (20210302124161, 20210302124689, 20210302124025).

#### References

- [1] Katori H, Ido T, Kuwata-Gonokami M. Optimal design of dipole potentials for efficient loading of Sr atoms. *J Phys Soc Japan* 1999;68:2479–82.
- [2] Barredo D, Lienhard V, Scholl P, de Léséleuc S, Boulier T, Browaeys A, et al. Three-dimensional trapping of individual Rydberg atoms in ponderomotive bottle beam traps. *Phys Rev Lett* 2020;124:023201.
- [3] Jau YY, Hankin AM, Keating T, Deutsch IH, Biedermann GW. Entangling atomic spins with a Rydberg-dressed spin-flip blockade. *Nature Phys* 2015;12:71–4.
- [4] Liu B, Jin G, He J, Wang J. Suppression of single-caesium-atom heating in a microscopic optical dipole trap for demonstration of an 852-nm triggered single-photon source. *Phys Rev A* 2016;94:013409.
- [5] Li G, Zhang S, Isenhower L, Maller K, Saffman M. Crossed vortex bottle beam trap for single-atom qubits. *Opt Lett* 2012;37:851–3.
- [6] Ye J, Kimble HJ, Katori H. Quantum state engineering and precision metrology using state-insensitive light traps. *Science* 2008;320:1734–8.
- [7] McKeever J, Buck JR, Boozer AD, Kuzmich A, Nagerl HC, Stamper-Kurn DM, et al. State-insensitive cooling and trapping of single atoms in an optical cavity. *Phys Rev Lett* 2003;90:133602.
- [8] Liu B, Jin G, Sun R, He J, Wang JM. Measurement of magic-wavelength optical dipole trap by using the laser-induced fluorescence spectra of trapped single caesium atoms. *Opt Express* 2017;25:15861–7.
- [9] Li L, Dudin YO, Kuzmich A. Entanglement between light and an optical atomic excitation. *Nature* 2013;498:466–9.
- [10] Takamoto M, Hong F-L, Higashi R, Katori H. An optical lattice clock. *Nature* 2005;435:321–4.
- [11] Dörscher S, Huntemann N, Schwarz R, Lange R, Benkler E, Lipphardt B, et al. Optical frequency ratio of a  $171\text{Yb}^+$  single-ion clock and a  $87\text{Sr}$  lattice clock. *Metrologia* 2021;58:015005.
- [12] McFerran JJ, Yi L, Mejri S, Di Manno S, Zhang W, Guéna J, et al. Neutral atom frequency reference in the deep ultraviolet with fractional uncertainty  $= 5.7 \times 10^{-15}$ . *Phys Rev Lett* 2012;108:183004.
- [13] Graham TM, Song Y, Scott J, Poole C, Phuttitarn L, Jooya K, et al. Multi-qubit entanglement and algorithms on a neutral-atom quantum computer. *Nature* 2022;604:457–62.
- [14] Porsev SG, Beloy K, Derevianko A. Precision determination of electroweak coupling from atomic parity violation and implications for particle physics. *Phys Rev Lett* 2009;102:181601.
- [15] Safronova MS, Safronova MS, Clark CW. Magic wavelengths, matrix elements, polarizabilities, and lifetimes of Cs. *Phys Rev A* 2016;94:012505.
- [16] Grimm R, Weidemüller M, Ovchinnikov YB. Optical dipole traps for neutral atoms. *Adv At Mol Opt Phys* 2000;42:95–170.
- [17] Kien FL, Schneeweiss P, Rauschenbeutel A. Dynamical polarizability of atoms in arbitrary light fields: general theory and application to cesium. *Eur Phys J D* 2013;67:92.
- [18] Mitroy J, Safronova MS, Clark CW. Theory and applications of atomic and ionic polarizabilities. *J Phys B Atomic Mol Phys* 2010;43(20):202001.
- [19] Šibalić N, Pritchard JD, Adams CS, Weatherill KJ. ARC: An open-source library for calculating properties of alkali Rydberg atoms. *Computer Phys Commun* 2017;220:319–31.
- [20] Robertson EJ, Šibalić N, Potvliege RM, Jones MPA. ARC 3.0: An expanded Python toolbox for atomic physics calculations. *Computer Phys Commun* 2021;261:107814.
- [21] Bai JD, Wang X, Hou XK, Liu WY, Wang JM. Angle-dependent magic optical trap for the  $6S_{1/2} \leftrightarrow nP_{3/2}$  Rydberg transition of cesium atoms. *Photonics* 2022;9:303.
- [22] Bai JD, Liu S, He J, Wang JM. Towards implementation of a magic optical-dipole trap for confining ground-state and Rydberg-state cesium cold atoms. *J Phys B: At, Mol & Opt Phys* 2020;53(15):155302.
- [23] Wang JY, Bai JD, He J, Wang JM. Realization and characterization of single-frequency tunable 637.2 nm high-power laser. *Opt Commun* 2016;370:150–5.
- [24] Bai JD, Wang JY, He J, Wang JM. Electronic sideband locking of a broadly tunable 318.6 nm ultraviolet laser to an ultra-stable optical cavity. *J Opt* 2017;19:045501.